A comprehensive mineralogical study of a jackstone calculus and some other human bladder stones from Campania Region (southern Italy)

Mercurio M.[1], Izzo F.[1*], Gatta G.D.[2], Salzano L.[3], Lotrecchiano G.[3], Germinario C.[1], Grifa C.[1], Varricchio E.[1], Langella A.[4]

[1]Dipartimento di Scienze e Tecnologie, Università degli Studi del Sannio, Via F. De Sanctis, 82100, Benevento, Italy

[2]Dipartimento Scienze della Terra, Università degli Studi di Milano, Via Botticelli 23, 20133, Milan, Italy

[3]UOC Urologia, Azienda Ospedaliera San Pio di Benevento, Via dell'Angelo 82100, Benevento, Italy

[4]Dipartimento di Scienze della Terra, dell'Ambiente e delle Risorse, Università degli Studi di Napoli Federico II, Complesso Universitario di Monte Sant'Angelo, Edificio 10, Via Vicinale Cupa Cintia 21, 80126 Naples, Italy

*Corresponding author. E-mail address: francesco.izzo@unisannio.it

Abstract

Keywords: bladder stones, jackstone calculus, sea-urchin appearance, EMPA-WDS, Weddellite,

Highlights

1. Introduction

Urolithiasis distresses Western population with an incidence of up to about 20%. The phenomenon has been addressed in medicine since the early 1800s, although evidence of a bladder stone dates back to the prehistoric period [1]. Nowadays, several studies have been published [2–12] and mostly conducted in order to contribute to the improvement of the clinical treatment of this painful pathology with impacting social and economic implications [13,14]. From an epidemiological point of view, in addition to the geographical location, other key factors to consider are: gender, race, age, familiarity, diet (included drinking water quality), smoking, climate, occupation and physical activity [15–18]. It is almost certain that most of the people suffering from this disease are white, males, between 40 and 50 years old, observing diets rich in animal proteins, sedentary and living in warm and humid regions [15,19]. Within this frame, Italian population seems to be particularly predisposed to such forms of urolithiasis (up to 9% of the population reports cases), as evidenced by an estimated incidence of 100k new cases per year stimulating the scientific community to always proceed to investigations taking into account the aforementioned key factors [20].

Main actors of urolithiasis are polyphasic biominerals mixed with organic phases consisting, as reported by Daudon et al. (2016) [11], of calcium oxalates, calcium phosphates, urates and uric acid, and other rare phases (e.g. cystine, proteins, purines or rare drugs).

Formation of urinary stones is determined by a combination of different processes, from supersaturation followed by nucleation, the latter enhanced by the activity of inhibitors (e.g. magnesium, citrate ions) and promoters (e.g. calcium, organic compounds such as cholesterol) [7,21]. Hence, the need to address the issue with a multidisciplinary approach: a new geobiological model on the dissolution of kidney stones *in vivo* has recently been proposed, shedding new light on clinical implications [22]. “Give me your stone, I will tell you who you are” was the title of an interesting study by Cloutier et al. (2015) [6], which highlighted the importance of a thorough analytical characterization at the basis of a correct aetiology, unveiling the minerogenetic processes

underlying kidney stones. This interesting approach highlights two important aspects: 1) which information from stone analysis could be clinically relevant and 2) the keys for interpretation of stone analysis. In other words, the urinary stone can be likely defined as an environmental geo-bio-marker and its in-depth analytical characterization may provide useful information regarding the anamnesis of the patient. To achieve this goal, the scientific community requires the application of an approach typical of mineralogical sciences, as suggested for the first time by Prien and Frondel (1947) [12]. Several analytical techniques have been used to acquire chemical, mineralogical and textural data for urinary stones: Scanning Electron Microscopy coupled with Energy Dispersive Spectroscopy or Wavelength Dispersive Spectroscopy analysis (SEM/EDS or WDS), X-ray Diffraction (XRD), Infrared spectroscopy (IR), thermal analyses, computed tomography, polarized light and stereoscopic microscopy, and image analysis [3,5–7,23–28]. Nevertheless, a limit to this approach is due to *i*) a usually low amount (few milligrams) of sample and *ii*) the lack of comprehensive and comparative studies reporting data from all the techniques above described. Actually, it is necessary to remark that a reliable laboratory analysis should provide, beyond a mineralogical classification, also a chemical characterization concerning the content of alkaline, earth-alkaline and heavy metals (e.g. Hg, As, Pb, Cd, etc.). In fact, it has been shown that trace elements can be markers of environmental risks also representative of the trigger factors involved in urinary stones formation [19,29–32].

Based on this premises and considering the very few studies giving information on bladder stones, especially indicative of Italian patients [20], the present research offers a multi-methodological approach aimed at a mineralogical characterization of a number of human bladder stones, available thanks to an active collaboration with the Department of Urology of *San Pio* Hospital in Benevento, Italy. The primary purpose of this investigation was to verify the existence of correlations between the studied biominerals and the association of major (> 1 wt.%) and trace (< 1 wt.%) elements, including “exotic” metals that can be crucial for the assessment of a potential environmental/food contamination.

1.1 The bladder stones

Most urinary stones are located in the kidney (kidney stones), but a small fraction (ca. 5%) grows inside the ureter and bladder, the latter called bladder stones. Those who suffer most are males from developed countries with a bimodal trend: children and adults over 60 years of age. According to EUA guidelines [33], bladder stones can be classified as primary, secondary or migratory, as a consequence of a multifactorial etiology. Primary bladder stones (also known as endemic bladder stones) are typically observed in children, in absence of urinary tract pathologies. Secondary bladder stones can be due to several causes, such as bladder outlet obstruction or other urinary tract abnormalities. In some cases, urinary stones that formed in the upper urinary tract can reach the bladder becoming a *nidus* for bladder stones (migratory bladder stones).

Bladder stones represent a non-negligible set of biominerals, having quite amazing features. Referring to the classification of urinary stones by Daudon et al. (2016)[11], there are seven morpho-constitutional types: type I (a, b, c, d, e) Calcium Oxalate Monohydrate (COM), type II (a, b, c) Calcium Oxalate Dihydrate (COD), type III (a, b, c, d) uric acid and urate, type IV (a1, a2, b, c, d) phosphate, type V (a, b) cystine, type VI (a, b, c) protein and Type VII miscellaneous stones.

Jackstone calculus, commonly reported in veterinary and rarely in human literature [34,35], is a rare bladder subtype of urinary stone with a sea-urchin appearance or resembling a toy jacks. It is almost always composed of calcium oxalate dehydrate, characterized by a dense central core and radiating spicules [36]. As far as investigation of Italian bladder stones are concerned, rare case studies have been reported so far [37], thus leaving some questions related to mineralogical aspects still debated.

2. Materials and methods

2.1 Biominerals

Bladder stone samples have been surgically collected from six male patients admitted to the Department of Urology of the *San Pio* Hospital (Benevento, Italy) in 2020. Clinical interviews were also held, in anonymous form, in order to gather some useful information about patient's medical history and lifestyle (Table 1). All the patients (67-76 years old) are resident in Campania region. Only one patient states to have a desk job, whereas the remaining ones are farmers or retired. None of the patients has a regular physical activity. Considering their body weight and height, the BMI (Body Mass Index) ranges from 25.3 (KS011B) and 29.4 (KS012B) that, according to the World Health Organization, define them as overweight. Furthermore, they suffer from a large variety of diseases such as diabetes (KS011B), arteriosclerotic heart disease (KS012B), dyslipidemia (KS020B) and hypertension (KS006B and KS023B). As far as eating habits are concerned, all patients state to get carbohydrates and protein foods (meat, eggs, and cheese) at least once per week or more, and less frequently vegetables. They also drink wine and coffee every day, and moderately beer and other alcohols. Only one patient drinks exclusively tap water (KS022B).

Table 1 - Patient's personal details. BMI, Body Mass Index.

n	ID	Gender	Age	Occupation	Physical activity	Body weight	Height	BMI	Weight of the calculus
1	KS006B	Male	76	Retired	no	78 kg	175 cm	25.5	1.09 g
2	KS011B	Male	75	Farmer	no	69 kg	165 cm	25.3	0.53 g
3	KS012B	Male	73	Farmer	no	90 kg	175 cm	29.4	1.55 g
4	KS020B	Male	67	Barman	no	78 kg	165 cm	28.6	1.05 g
5	KS022B	Male	76	Farmer	no	74 kg	170 cm	25.6	3.15 g
6	KS023B	Male	75	Employed	no	75 kg	165 cm	27.6	9.75 g

Bladder stones were selected as a function of the availability of material (weight ranging from 0.5 g to 9.7 g) in order to ensure a complete chemical, mineralogical and petrographic characterization.

Before the analyses, bladder stones have been washed thoroughly with distilled water, sterilized in pure ethanol and then dried at room temperature.

2.2 Lab strategy

Preliminary morphological description of bladder stones has been carried out by means of a NIKON SMZ 1000 stereomicroscope connected to a NIKON digital Sight DSRi2 camera. Polarized Light Microscopy (PLM) observations carried out on thin sections (ca. 30 μm) using a Nikon Eclipse 6400 POL microscope equipped with a Nikon DS-Fi camera provided information on the microtextural features and the mineralogical composition of the bladder stones. Chemical phases were also detected by Fourier Transform Infrared Spectroscopy (FTIR) performed in Attenuated Total Reflectance mode (ATR) by means of a Bruker ALPHA-R spectrometer (Bruker Opus 7.0 software) in the mid-infrared spectral range (4000–400 cm^{-1}, 64 scans, 4 cm^{-1} resolution).

For a crystalline phase identification of the aforementioned samples, X-ray powder diffraction data were collected at the XPRESS beamline of the ELETTRA Synchrotron radiation facility (Trieste, Italy) [38]. Data collections were performed by a monochromatic and polarized circular beam, with a wavelength of 0.4957 Å and a diameter of ca. 50 μm. Powder samples were loaded in B-glass capillaries (300 μm in diameters). A MAR345 image plate detector was used, positioned at 340 mm from the sample. The following collection strategy was adopted: the capillary was rotated from -5 to +5 ° around the (vertical) ω -axis for an exposure time of 60 s. The 2D powder diffraction rings, collected in transmitting geometry, were converted into 2-theta *vs.* intensity plots, using the Fit2D software [39]. Geometrical parameters were previously refined based on the XRD pattern of the LaB_6 calibrant. The preliminary identification of the crystalline components was performed using the suite of programs X'Pert-HighScore (Panalytical).

Major and trace elements were quantitatively detected via electron-microprobe analyses obtained from polished and carbon-coated sections using a JEOL JXA-8200 microprobe in wavelength dispersive mode (EMPA/WDS). The system was operated using an accelerating voltage of 15 kV, a

counting time of 30 s on the peaks and 10 s on the backgrounds. The following standards were used: Na (omfacite), Sr (celestine), Mn (rodonite), K (K-feld), Mg (forsterite-154), As (niccolite), Hg (HgSe), Fe (fayalite-143), Ca (grossularia), Al (grossular), Se (HgSe), Cd (metal), Ni (niccolite), Pb (galena), P (apatite), Sb (metal), Cu (e metal), Cr (metal), Zn (metal).

The thermal behavior of bladder stones was investigated by Simultaneous Thermal Analyses (STA) TG-DSC (NETZSCH STA 449 F3 Jupiter) coupled with a FTIR BRUKER Tensor 27 for the Evolved Gas Analysis (EGA) by a transfer line heated at 200 °C. The samples were heated from 40 °C to 1050 °C, with a heating rate of 10 °C/min in pure air atmosphere (flow rate 60mL/min). TG and DSC curves were processed with the NETZSCH Proteus 6.1 Software.

3. Results

3.1 Under microscope

3.1.1 Stereomicroscopy

The observation of urinary stones by means of a stereomicroscope represents a first fundamental approach in their characterization, providing important information in terms of etiological or pathophysiological conditions [11]. This examination is based on a morphological evaluation of the aggregates, taking into account color, shape, aspect of the surface and the section, presence of umbilication (papillary imprint) and Randall's Plaque [40–42].

Fig. SM reports selected micrographs of the examined bladder stones. KS006B shows a light colored rough surface with radial crystallization and not well-defined concentric layers in the inner part (**Fig. SMa and b**). Sample KS011B shows an orange, compact and concentric microstructure with a radiating organization, interested by sporadic brownish intercalations. This sample exhibits a homogeneous smooth surface (**Fig. SMc**). KS012B displays a sea-urchin appearance and a particular brown spiculated surface (**Fig. SMd**), with a finely granular and poorly organized section (**Fig. SMe**). In KS020B, the brown-orange concentric structure is poorly organized with thin porous

and orange layers (**Fig. SMf, g and h**). A heterogeneous coloration, from beige to brown-orange, is observed for the rough surface of KS022B, which clearly shows an orange concentric structure with radial organization (**Fig. SMi and j**). Lastly, the fragments forming KS023B exhibit a compact concentric internal structure with a radiating organization, along with frequent small orange-brown inclusions (**Fig. SMk**). The color is not homogeneous, ranging from pale yellow to whitish. A quite smooth surface can be also observed (**Fig. SMl**).

3.1.2 Polarized light microscopy

Further information about the internal microstructure and mineralogical nature for the examined bladder stones can be inferred by means of Polarized Light Microscopy (PLM). In order to describe shape, size and optical properties (birefringence, cleavage, extinction, etc.) of mineralogical species, bladder stones were thin-sectioned parallel to the concentric layers, in order to investigate even the central portion of the samples, where the *nuclei* usually occur.

The sea-urchin appearance of KS012B is still recognizable in thin section (**Fig. PLMa**). The internal concentric pattern of this sample appears well-defined but irregular and poorly organized, suggesting the occurrence of different nucleation centers. It is composed by subhedral or anhedral crystals with high interference colors (**Fig. PLMb**), consistent with the optical properties of calcium oxalate (i.e., whewellite) aggregates [20,43].

KS006B displays a weakly consistent internal structure made of acicular crystal of brushite (**Fig. PLMc**). This mineral species shows a low surface relief, a perfect cleavage and first order interference colors [44]. Furthermore, this aggregate is interested by the presence of darker layers, likely made of amorphous/organic substances.

The remaining samples (KS011B, KS020B, KS022B and KS023B) are generally similar each other as they exhibit a more or less compact concentric structure, with colors ranging from dark brown to pale yellow. In crossed polars, the aggregates display not well-defined interference colors, ranging from grayish to yellowish. These features are usually consistent with uric acid aggregates [20,45].

3.3 FTIR

FTIR measurements on bulk powdered samples provide a first reliable characterization, at the atomic scale, of urinary stones [2,3,10,23,46–51]. Absorption bands of the bladder stones examined in the present investigation are summarized in **Table FTIR**, whereas in **Fig. FTIR** their FTIR spectra (ATR mode) are shown. Excluding some shared signals, the results clearly highlighted the compositional differences between the analyzed biominerals.

Samples KS011B, KS020B, KS022B and KS023B display the same pattern, fully compatible with that of uric acid $C_5H_4N_4O_3$ [10]. Particularly interesting are the absorption bands assigned to N-H stretching vibrations [49,51], such as those at ca. 3086 cm^{-1}, 2994 cm^{-1}, 2915 cm^{-1}, 2788 cm^{-1}, 2685 cm^{-1} and 2604 cm^{-1} standing on a broad band between 3300-2800 cm^{-1}. The remaining absorption bands describe a very dense sequence of narrowed signals in the fingerprint region, approximately between 1800-400 cm^{-1} (**Fig. FTIR**).

Different spectroscopic features were observed for the samples KS006B and KS012B. The former shows the typical FTIR spectrum of the mineral brushite $CaHPO_4 \cdot 2(H_2O)$ [52–54]. As a whole, the absorption bands at higher wavenumbers indicate the stretching (3542 cm^{-1} and 3474 cm^{-1}) and bending (1664 cm^{-1}) vibrations of H_2O molecules. On the other hand, absorption bands in the fingerprint region are mainly due to the HPO_4 group. The peak at 1205 cm^{-1} is assigned to H-in plane bending vibration, whereas the signals at 1135 cm^{-1}, 1059 cm^{-1}, 986 cm^{-1} and 872 cm^{-1} are due to P-O stretching vibrations. The bands at 577 cm^{-1} and 523 cm^{-1} could be ascribed to the O-P-O bending vibrations. In spite of the high correlation of the FTIR spectrum of the sample KS006B with those reported in literature [52–54], some bands in the fingerprint region did not perfectly fit the typical expected wavenumbers. This mismatch is likely due to some ionic substitutions or to the occurrence, in this sample, of other chemical compounds. Moreover, the additional occurrence of a band at 1323 cm^{-1} (**Table FTIR**) is probably due to the presence of CaOx inclusions.

As far as sample KS012B is concerned, FTIR measurements suggest the typical composition of a calcium oxalate [49,50,55]. The main diagnostic bands of this species lie at ca. 1610 cm^{-1} (C=O vibration), 1313 cm^{-1} (C-O vibration), 886 cm^{-1} (C-C stretching), 779 cm^{-1} (C-H bending), 656 cm^{-1} (O-H bending), 511 cm^{-1} (in-plane O-C=O bending). Spectra also showed a sequence of absorption bands at higher wavenumbers (3440 cm^{-1}, 3318 cm^{-1}, 3225 cm^{-1} and 3043 cm^{-1}), generally ascribable to symmetric and asymmetric O-H stretching vibrations. According to the previous experimental findings [56], the high intensities of the absorption bands at 779 cm^{-1} and 511 cm^{-1} allow to infer the occurrence, in sample KS012B, of the mineral whewellite (calcium oxalate monohydrate $CaC_2O_4 \cdot H_2O$). Lastly, a very weak absorption band at ca. 1044 cm^{-1} can be also observed (**Table FTIR**).

Table FTIR: FTIR data of bladder stones (expressed in cm^{-1}). Note: br = broad; vs = very strong; s = strong; sh = shoulder; m = medium; w = weak; n.d. = not determined.

KS006B	KS011B	KS012B	KS020B	KS022B	KS023B	Chemical phase
3542 w						Brushite
3474 w						Brushite
		3440 w				Calcium oxalate
3268 w						Brushite
		3318 w				Calcium oxalate
		3225 w				Calcium oxalate
3155 w						Brushite
	3089 sh		3084 sh	3082 sh	3088 sh	Uric Acid
		3043 w				Calcium oxalate
	2983 m		2996 m	2992 m	3005 m	Uric Acid
	2918 w		2912 w	2914 w	2917 w	Uric Acid
	2788 m		2785 m	2787 m	2793 m	Uric Acid
	2687 m		2680 m	2687 m	2684 m	Uric Acid
	2605 sh		2609 sh	2600 sh	2603 sh	Uric Acid
	1661 vs		1654 vs	1662 vs	1662 vs	Uric Acid
1644 w						Brushite
		1610 vs				Calcium oxalate
	1584 s		1585 s	1584 s	1585 s	Uric Acid
	1435 m		1434 m	1435 m	1435 m	Uric Acid
	1398 m		1399 m	1399 m	1399 m	Uric Acid
		1380 vw				Calcium oxalate
	1347 m		1347 m	1347 m	1347 m	Uric Acid
1323 vw						Calcium oxalate
		1313 vs				Calcium oxalate
	1301 m		1302 m	1301 m	1302 m	Uric Acid
1205 m						Brushite
1135 m						Brushite
	1121 m		1121 m	1121 m	1121 m	Uric Acid
1059 s						Brushite
		1044 vw				n.d.
	1025 w		1026 w	1025 w	1026 w	Uric Acid
	990 m		990 m	990 m	990 m	Uric Acid
986 m						Brushite
		952 vw				Calcium oxalate
		886 w				Calcium oxalate
872 w	875 w		876 w	875 w	875 w	Uric Acid/Brushite
784 w	779 m	779 vs	781 m	779 m	780 m	Uric Acid/Calcium oxalate/Brushite
	742 s		743 s	742 s	743 s	Uric Acid
	703 s		702 s	703 s	703 s	Uric Acid
655 vw		656 m				Calcium oxalate/Brushite
	617 m		617 m	617 m	617 m	Uric Acid
		597 m				Calcium oxalate
577 w	572 m		572 m	571 m	572 m	Uric Acid/Brushite
523 vs	519 m		519 m	520 m	520 m	Uric Acid/Brushite
		511 s				Calcium oxalate
	470 vs		471 vs	469 vs	470 vs	Uric Acid

3.4 Synchrotron X-ray Diffraction (XRD)

The X-ray diffraction patterns (2-theta range: 3 – 40°, λ = 0.4957 Å) were successfully indexed and ascribed to the following crystalline species (**Fig. XRD-1**):

- KS006B is substantially composed by brushite [$Ca(HPO_4)\cdot 2H_2O$, $a \cong 6.36$, $b \cong 15.19$, $c \cong 5.81$ Å, $\beta \cong 118.4°$, sp. gr. $C2/c$] and weddellite [$CaC_2O_4\cdot(2.5\text{-}x)H_2O$, $a \cong 12.37$, $c \cong 7.36$ Å , sp. gr. $I4/m$], and minor evidence ascribable to the presence of whewellite [$CaC_2O_4\cdot H_2O$, $a \cong 6.29$, $b \cong 14.58$, $c \cong 10.12$, $\beta \cong 109.46$, sp. gr. $P2_1/c$] are observed (**Fig. XRD-2**). In particular, the most intensive peak of whewellite (at 2-theta ≅ 4.753°) lies on the shoulder of the most intensive peak of weddellite (at 2-theta ≅ 4.576°);
- KS011B is substantially composed by uric acid [$C_5H_4N_4O_3$, $a \cong 14.46$, $b \cong 7.40$, $c \cong 6.21$ Å, $\beta \cong 65.10$ °, sp. gr. $P2_1/a$];
- KS012B is composed by whewellite;
- KS020B is substantially composed by uric acid (only very minor evidence, potentially ascribable to the presence of whewellite, can be considered);
- KS022B is substantially composed by uric acid (only very minor evidence, potentially ascribable to the presence of whewellite, can be considered);
- KS023B is substantially composed by uric acid (only very minor evidence, potentially ascribable to the presence of whewellite, can be considered);

The full-width-at-half-maximum (FWHM, estimated by Le Bail full-profile fit; [57]) of the brushite peaks is about 0.22°, whereas the diffraction peaks of uric acid (FWHM ≅ 0.14°) and weddellite (FWHM ≅ 0.15°) are significantly sharper.

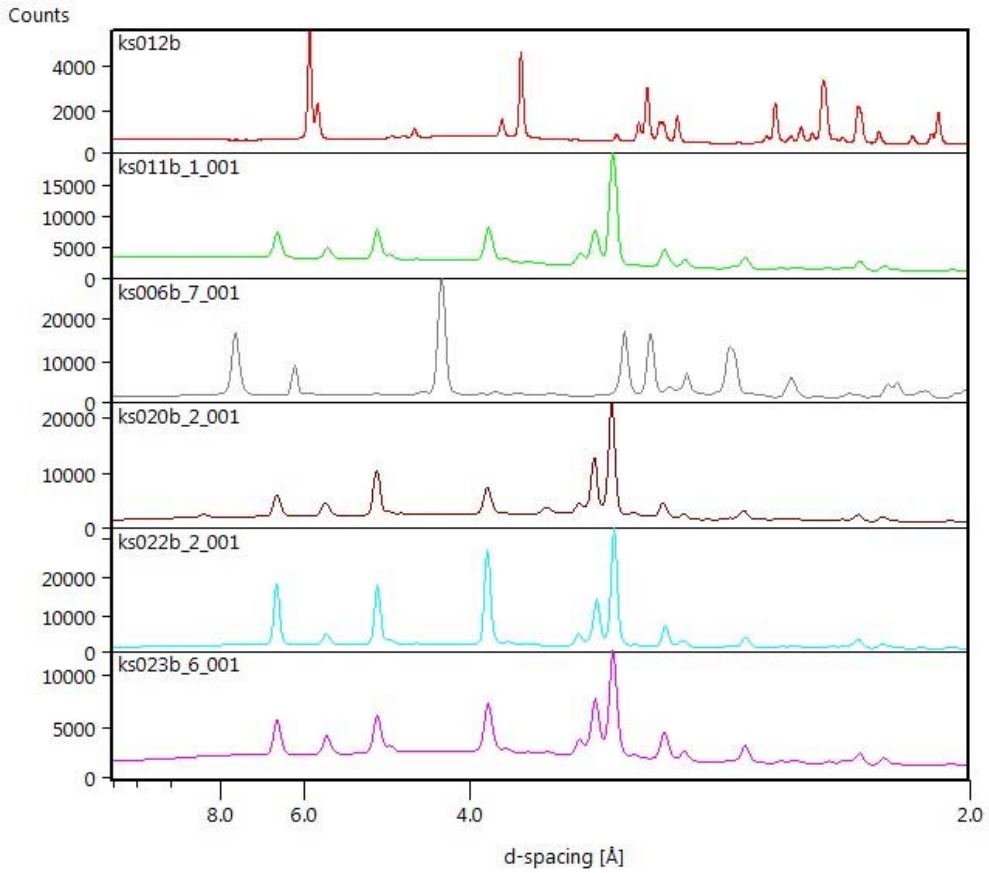

Fig. XRD-1. Synchrotron X-ray powder diffraction patterns [*d*-spacing (Å) *vs.* intensity (counts)] pertaining to the samples KS006B, KS011B, KS012B, KS020B, KS022B and KS023B (λ = 0.4957 Å).

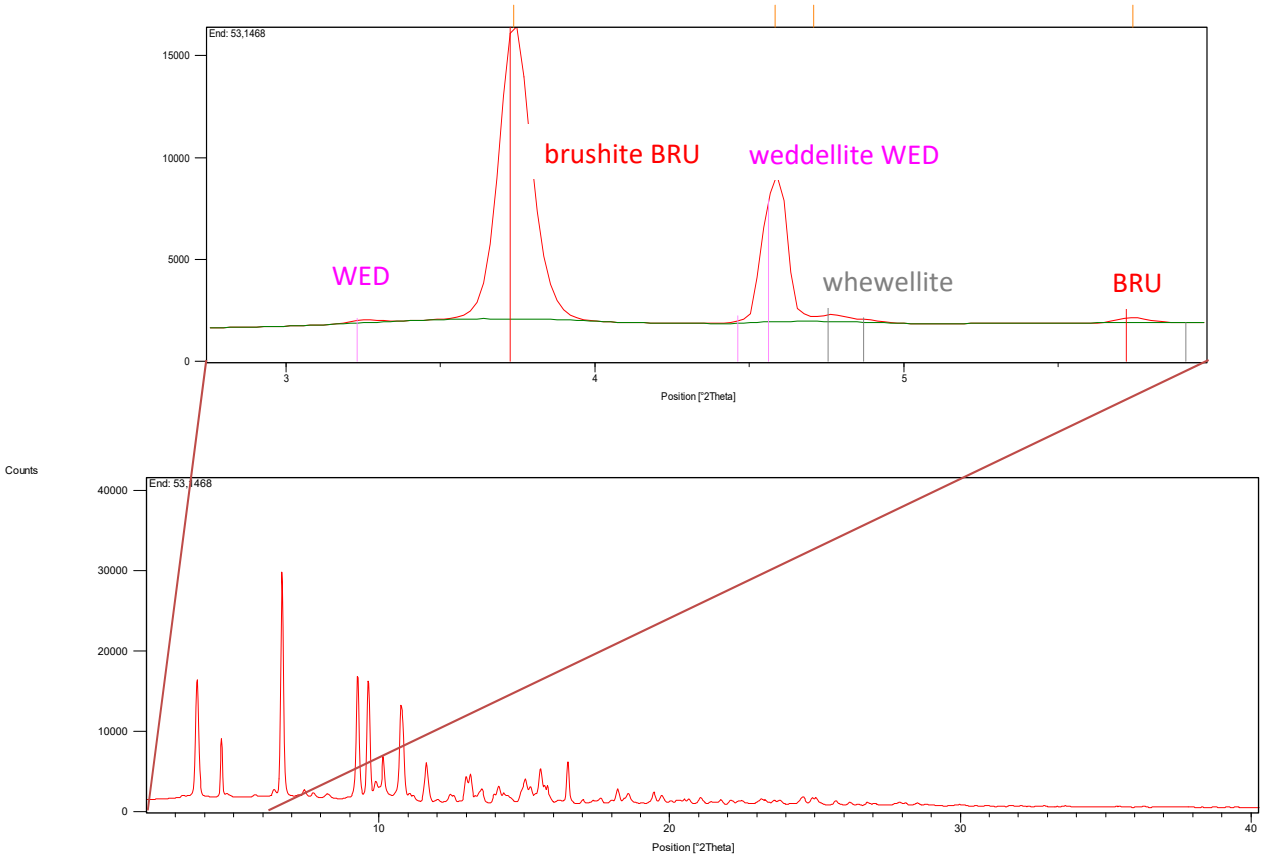

.

Fig. XRD-2: X-ray diffraction pattern pertaining [2-theta (°) *vs.* intensity (counts)] to the sample KS006B, and zoom of the low-theta region (λ = 0.4957 Å). Red bars: brushite, purple bars: weddellite, grey bars: whewellite

3.5 EMPA/WDS

Chemical data here provided (**Table EMPA**) reflect the occurrence and relative concentration of both major and some peculiar trace elements, as well as their distribution in the bladder stones. Although mainly formed by brushite, as detected by FTIR and XRD analyses, chemical and mineralogical composition of sample KS006B appears quite heterogeneous in EMPA/WDS (**Fig. EMPA**), showing the occurrence of acicular and radiating crystals of brushite (Ca ~23.5 wt.%, P ~18.0 wt.%), along with bipyramidal crystals of calcium oxalate (Ca ~30.9 wt.%) (**Table EMPA**). This bladder stone also displays the occurrence of spheroidal particles (< 10 μm) composed by calcium (~32.25 wt.%) and phosphorous (~17.5 wt.%), characterized by an internal concentric structure and mainly located into the cavities (**Fig. EMPA**).

Ca-phosphate inclusions (Ca, 33.83 wt.%; P, 15.70 wt.%) can be also observed for the sea-urchin calculus (KS012B), at the interface between its internal multinucleus structure and the external budding surface (**Fig. EMPA**). The remaining part of this bladder stone is composed by calcium oxalate (Ca ~30.23 wt.%) (**Table EMPA**).

Inclusions of Ca-oxalate and Ca-phosphate in uric acid bladder stones (KS011B, KS020B, KS022B and KS023B) are scattered along the layers forming the internal concentric structure (**Fig. EMPA**). In sample KS011B, a compact layer of calcium oxalate is clearly observed between uric acid levels (**Fig. EMPA**).

As far as trace elements are concerned, the occurrence of alkali metals such as Na and K can be observed in all the mineral species forming the examined samples (**Fig. EMPA map and Table EMPA**). Nevertheless, their concentration in Ca-phosphate inclusions was generally higher than those measured in oxalates and uric acids. The same goes for the alkali-earth metal Mg and transition metal Zn, whereas Sr is generally more abundant in calcium oxalates. Iron, and less frequently Mn, is mainly concentrated in Ca-P and Ca-Ox phases. Aluminum and antimony were also detected in most of analyzed points, whereas nickel was only found in sample KS012B (CaOx urolith) and Ca-P scattered inclusions of sample KS023B (uric acid). Traces of Pb were also found

in all samples, sometimes along with other heavy metals such as Cr, Cd and Hg. Chromium and mercury were found only in oxalates (scattered inclusions) and uric acids, as well as arsenic and selenium. The latter was detected only in uric acid bladder stones, except for sample KS011B and the outer part of sample KS020B (**Table EMPA**). It is worth to note also the sporadic occurrence of copper in some uric acids (KS011B, KS020B and KS023B) and CaOx (KS012B).

Table EMPA: Average concentration of major (>1 wt.%, in bold) and trace elements (<1wt.%) detected for bladder stones by EMPA/WDS. Main mineral species (*), standard deviation (σ), detection limits (D.L.), number of analyzed points and measurements are also reported.

Sample ID	Chemical phase		Ca	P	Na	K	Zn	Pb	Sr	Mg	Cr	Mn	Fe	Ni	Cu	Al	Cd	Sb	As	Se	Hg
	Brushite*	wt.%	**23.536**	**17.986**	0.063	0.034	0.109	0.057		0.024											
	(5 points)	σ	0.402	0.329		0.002	0.051	0.011		0.004											
		D.L.	0.014	0.027	0.015	0.010	0.056	0.027		0.014											
		meas.	5	5	1	3	3	2		3											
KS006B	Ca-Oxalate	wt.%	**30.954**	0.148	0.068	0.021	0.077	0.039	0.064		0.039		0.042					0.064			0.072
(16 points)	*(scattered inclusions)*	σ	0.350	0.013	0.027	0.006		0.036					0.017					0.015			
	(5 points)	D.L.	0.014	0.021	0.015	0.010	0.052	0.029	0.035		0.028		0.025					0.043			0.068
		meas.	5	5	4	4	1	2	1		1		2					3			1
	Ca-Phosphate	wt.%	**32.253**	**17.472**	0.764	0.186	0.236	0.037	0.063	0.505		0.033	0.042			0.030	0.045	0.058			
	(spheroidal particles)	σ	0.556	0.412	0.144	0.013	0.064	0.002		0.047		0.007	0.018			0.007	0.008				
	(6 points)	D.L.	0.015	0.026	0.019	0.011	0.057	0.030	0.046	0.015		0.027	0.027			0.014	0.030	0.045			
		meas.	6	6	6	6	5	2	1	6		2	2			2	2	1			
	Uric acid*	wt.%	0.031	0.034	0.033	0.023	0.043	0.038		0.017		0.020	0.019		0.041	0.015	0.040				0.086
	(5 points)	σ	0.025		0.012	0.007		0.019		0.009			0.010				0.001				
		D.L.	0.008	0.017	0.013	0.007	0.037	0.021		0.012		0.017	0.018		0.026	0.010	0.023				0.050
		meas.	4	1	3	5	1	2		2		1	2		1	1	2				1
KS011B	Ca-Oxalate	wt.%	**29.162**	0.161	0.170	0.026	0.057	0.032	0.172	0.028			0.042			0.057	0.041	0.044	0.040		
(17 points)	*(layer)*	σ	1.029	0.027	0.040	0.006	0.001		0.030	0.015						0.060					
	(6 points)	D.L.	0.014	0.021	0.016	0.010	0.051	0.029	0.052	0.013			0.026			0.013	0.031	0.043	0.034		
		meas.	6	6	6	5	2	1	2	4			1			3	1	1	1		
	Ca-Oxalate	wt.%	**28.675**	0.171	0.157	0.020	0.066	0.039		0.017		0.032	0.041			0.032					
	(scattered inclusions)	σ	0.583	0.020	0.020	0.006	0.010			0.003		0.005				0.032					
	(6 points)	D.L.	0.014	0.021	0.018	0.010	0.054	0.027		0.014		0.023	0.025			0.013					
		meas.	6	6	6	6	3	1		4		2	1			3					
	Ca-Oxalate*	wt.%	**30.228**	0.384	0.101	0.035	0.084	0.035	0.131	0.035	0.043	0.026	0.034	0.030	0.051	0.034	0.048	0.067			
	(19 points)	σ	0.929	0.120	0.028	0.014	0.019	0.007	0.051	0.018	0.010		0.006	0.001	0.016	0.014		0.006			
		D.L.	0.014	0.022	0.017	0.010	0.050	0.030	0.056	0.013	0.027	0.023	0.026	0.029	0.039	0.012	0.028	0.042			

KS012B		meas.	19		19	19	7	4	4	16	3	1	4	3	3	12	1	2				
(22 points)	Ca-Phosphate	wt.%	**33.827**	**15.697**	0.852	0.185	0.203	0.112	0.105	0.409				0.036								
	(scattered inclusions)	σ	2.164	2.735	0.068	0.011	0.013			0.009				0.004								
	(3 points)	D.L.	0.015	0.027	0.022	0.011	0.059	0.030	0.054	0.015				0.033								
		meas.	3	3	3	3	3	1	1	3				2								
	Uric acid*	wt.%	0.054	0.020	0.212	0.130	0.043	0.041	0.097	0.029					0.038	0.038						
	(outer part)	σ	0.027	0.002	0.045	0.021										0.025						
	(4 points)	D.L.	0.009	0.019	0.015	0.007	0.036	0.023	0.050	0.011					0.028	0.011						
KS020B		meas.	4	2	4	4	1	1	1	1					1	3						
(12 points)	Uric acid*	wt.%	0.018	0.023	0.033	0.033	0.056	0.052	0.085	0.014	0.034	0.018			0.041	0.04	0.026	0.029	0.039	0.041	0.099	
	(inner part)	σ	0.004	0	0.009	0.012	0.006		0.027	0.004						0.009					0.003	
	(8 points)	D.L.	0.008	0.017	0.016	0.007	0.036	0.020	0.041	0.011	0.019	0.017			0.026	0.010	0.022	0.027	0.026	0.021	0.048	
		meas.	8	2	4	8	2	1	2	2	1	1			1	4	1	1	1	1	2	
	Uric acid*	wt.%	0.024	0.027	0.028	0.024	0.064	0.034	0.084	0.015	0.026	0.019	0.018			0.043	0.027			0.029	0.061	
	(11 points)	σ	0.007	0.006	0.009	0.006	0.035	0.009	0.027	0.005	0.002					0.037	0.006				0.005	
		D.L.	0.009	0.018	0.015	0.008	0.038	0.021	0.046	0.010	0.019	0.017	0.017			0.010	0.023			0.023	0.052	
KS022B		meas.	11	4	7	11	2	3	3	4	2	1	1			3	2			1	3	
(13 points)	Ca-Oxalate	wt.%	**30.22**	0.246	0.161	0.02	0.116			0.025	0.029		0.042			0.067						
	(scattered inclusions)	σ	1.329	0.064	0.001	0.006	0.014			0.005												
	(2 points)	D.L.	0.014	0.023	0.017	0.010	0.048			0.014	0.028		0.026			0.012						
		meas.	2	2	2	2	2			2	1		1			1						
	Uric acid*	wt.%	0.021	0.025	0.021	0.035	0.039	0.046	0.094	0.013	0.031	0.021			0.035			0.043	0.027	0.03	0.084	
	(6 points)	σ	0.004		0.004	0.02			0.005			0.005							0.013			
		D.L.	0.008	0.017	0.015	0.007	0.033	0.021	0.050	0.010	0.019	0.017			0.026			0.028	0.030	0.026	0.054	
		meas.	5	1	4	6	1	1	2	1	1	2			1			1	2	1	1	
KS023B	Ca-Oxalate	wt.%	**29.272**	0.407	0.092	0.016	0.051	0.035	0.064	0.025			0.041		0.041	0.022		0.033			0.081	
(13 points)	*(scattered inclusions)*	σ	10.023	0.144	0.02	0.002				0.009			0.01									
	(5 points)	D.L.	0.014	0.020	0.016	0.010	0.041	0.030	0.046	0.013			0.024		0.032	0.011		0.032			0.079	
		meas.	5	5	5	3	1	1	1	5			3		1	1		1			1	
	Ca-Phosphate	wt.%	**17.895**	**9.055**	0.737	0.076	0.181	0.067	0.074	0.168		0.023	0.61	0.026		0.042	0.037					

(scattered inclusions)	σ	11.773	6.682	0.456	0.007	0.022			0.108			0.31			
(2 points)	D.L.	0.012	0.025	0.021	0.008	0.055	0.030	0.061	0.015	0.019	0.026	0.024	0.013	0.028	
	meas.	2	2	2	2	2	1	1	2	1	2	1	1	1	

3.6 Thermal behavior

A discrimination between anhydrous and hydrated phases occurring in the aggregates forming urinary stones is easily performed by following their thermal transformations recorded in STA analysis [5,23,51,58–64]. The TG curve of acid uric (samples KS011B, KS020B and KS023B) shows a unique event mainly consisting in a thermal decomposition of $C_5H_4N_4O_3$ occurring in the range 300-700 °C, with a maximum decomposition rate at around 430 °C and the consequent emission of complex mixtures of carbon dioxide and other nitrile compounds (**Fig. STA**). TG curves also show residual masses between 1-3 wt.%, due to the presence of impurities such as calcium oxalate and non-stoichiometric phosphates. This information was also confirmed by FTIR analyses carried out on the residues (**Suppl. Material**), which showed the occurrence of calcium monoxide (sharp absorption band at ~3640 cm^{-1} and a broader one at ~1410 cm^{-1}) [65,66] and calcium carbonate (~1412, ~873, and ~711 cm^{-1}) [67] as decomposition products of oxalate [68]. Thermal decomposition of phosphates also accounts for the formation of hydroxyapatite (~1016, ~958 and ~565 cm^{-1}) [66].

Thermal analyses of sample KS012B (**Fig. STA**) show the typical decomposition of calcium oxalate characterized by three well-defined thermal endothermic events [68]. The first one is due to the dehydration of $CaC_2O_4 \cdot H_2O$ at around 175 °C with a weight loss of ~13 wt.%. During the second event (~495 °C; ~19.5 wt.%), the decomposition of CaC_2O_4 leads to the formation of $CaCO_3$ and the concomitant release of CO (**Fig. STA**). Nevertheless, as a consequence of the disproportionation reaction $2CO \rightarrow CO_2 + C$, EGA also shows the simultaneous occurrence of carbon dioxide. At ~750 °C, $CaCO_3$ decomposes to form CaO and CO_2 (weight loss ~29 wt.%) (**Suppl. Material**).

Thermal transformation of sample KS006B (**Fig. STA**) reflects a two-steps dehydration of $CaHPO_4 \cdot 2H_2O$; the first one, within 300 °C (~162 and ~197 °C; weight loss ~20 wt.%), forms the mineral monetite $CaHPO_4$ [69–72], as well as the dehydration of oxalate impurities. Between 300-550 °C, a weight loss of about 6 % indicates the complete dehydration of monetite that leads to the

formation of a calcium pyrophosphate $Ca_2P_2O_7$. During this step, thermal decomposition of calcium oxalate also occurs with emission of CO and CO_2 as recorded by EGA. An additional weight loss (~2.5 wt.%) between 550-800 °C, with emission of CO_2, also occurs by dissociation of calcium carbonate, previously formed by decomposition of calcium oxalate. The presence of oxalate impurities along with monetite and calcium pyrophosphate was ascertained by means of FTIR analyses carried out on the residues after each thermal treatment (**Suppl. Material**).

4. Discussion

4.1 Morpho-constitutional classification

The chemical and mineralogical composition, coupled with the petrographic features, of urinary calculus allows to trace a classification on a morpho-constitutional basis, usually correlated to the specific patho-physiological conditions responsible for urolithiasis [6,11,73], essential to choice the best therapeutic strategy [74–76]. Following the classification proposed by Daudon et al. (2016)[11], further subgroups can be distinguished by a morphological observation of the surface of the stone: aspect of the section, characteristics of the *nuclei*, presence of Randall plaque, etc. Excluding the minor amounts of calcium oxalate inclusions and non-stoichiometric phosphate species detected (**Table FTIR, Table EMPA and Fig. EMPA**), the samples KS011B, KS020B KS022B, KS023B belong to the Type III (uric acids), while the KS006B and KS012B belong to the Type IV (brushite) and Type classes I/II (CaOx stones), respectively.

The compact and concentric microstructure of the samples KS011B and KS023B, along with a quite smooth surface, allow to assign them to the morphological subtypes IIIa (anhydrous uric acid), usually observed for older men affected by bladder urolithiasis, especially when interested by prostate hypertrophy [6,11]. Sample KS011B also displays the typical orange surface due to the presence in the urine of the red pigment uricine, easily trappable in the uric acid crystals, poorly adsorbed by the surface of sample KS023B as evidenced by the lighter shade, ranging from pale yellow to whitish. The poorly organized, porous internal microstructure of KS020B accounts for the

subtype IIIb (uric acid dihydrate). Lastly, sample KS022B presented at the same time an internal, concentric and compact structure (Type IIIa) and a rough surface (Type IIIb). This transition (Type IIIa -> Type IIIb) could be due to a progressive decrease of the urine pH (<5.5) and the consequent formation of uric acid dihydrate in the external parts of the bladder stone. The formation of uric acid-based bladder stones is often associated, in addition to the reduction of pH levels in the urine and their prolonged stasis often linked to benign hypertrophy of the prostate, also to hyperuricosuria, as well as to eating and metabolic disorders (the patient KS011B suffers from diabetes) [6,11]. Actually, in overweight subjects, uric acid and oxalate stones are often found. According to recent studies, there seems to be a relationship between calcium excretion and BMI. Calcium excretion could also justify the appearance of CaOx and CaP inclusions. This condition is supported in this study as all patients have a medium-high BMI index.

KS006B is a Type IVd calculus, as mainly formed by brushite and characterized by the occurrence of rod-shaped crystals arranged in a radial internal microstructure, with scarcely defined concentric patterns. Surface is rough and dappled. This kind of bladder stone is usually considered as idiopathic, namely related to unknown causes, although often observed in patients affected by primary hyperparathyroidism, hypercalciuria and medullary sponge kidney [9,77]. Considering the high recurrence rate of these stones and their resistance to extracorporeal shock wave lithotripsy (ESWL), patients affected by brushite nephrolithiasis usually require more aggressive clinical treatments [11]. KS006B also shows the occurrence of inclusions of CaOx (mainly weddellite) and spheroidal particles of non-stoichiometric and amorphous CaP stones, located as concentric layers in the porous system of brushite aggregate. It is possible that the latter inclusions act as precursors for apatite stones and the higher content of calcium could deal with the composition of amorphous calcium phosphate and/or rarer CaP phases, indicating hypercalciuria or urinary tract infection [11] and indicative of recent lithogenic processes [6]. Morphological features of these spherical inclusions remind those of some common inorganic mineral concretions (i.e., ooids) generally formed in subaqueous environments. It is possible that the mechanism of formation of these

inclusions was due to the interaction of supersaturated urine through the porous system of brushite, with a consequent release of calcium phosphate around a starting *nucleus* [20]. The tendency to form a perfect sphere could be strictly related to kinetic energy of the urine flow and/or steric effects between CaP inclusions [78].

Sample KS012B shows a spiculated appearance that allow us to classify this stone among the so-called *Jackstone calculi* [34,36,37,79–82]. This kind of urinary stone is freely movable in the bladder and is usually composed, according to literature [34,37,82], by calcium oxalate dehydrate. Considering the mineralogical composition and the poorly organized internal microstructure and the spiculated surface, sample KS012B generally accounts for Type I/II urinary stone, typical of weddellite/weddellite aggregates. It is possible that calcium oxalates, initially hydrate, converted to more stable mineralogical (anhydrous) phases [20,55,83].

4.2 Assumption on meaning of major and trace elements

The role of major and trace elements in the pathogenesis of urinary stones was widely investigated in the last decades, encouraging the use of these biominerals for biomonitoring purposes [7,30,84,85]. In particular, major and trace elements naturally occur in biocrystals as a consequence of food intake, metabolic processes and environmental factors. However, part of the trace elements can be accidentally incorporated into urinary stones, after a temporary storage in the kidneys, and can sometimes even affect the formation of crystals, thus acting as promoter or inhibitor agents [7,30,86].

The most relevant element for the lithogenesis of urinary stones is doubtless calcium, which occurs in the present study as major element in CaOx and CaP uroliths (either as dominant mineralogical species/minor inclusions; **Table Y**), or trace elements in uric acids. It is widely accepted that Ca can significantly influence the distribution of other trace elements, promoting the new crystallization processes in kidney or bladder [21]. In calcium-bearing phases forming uroliths, this element can be

partially replaced by substituent ions as sodium, magnesium or strontium, the latter particularly observed in CaOx phases. Since magnesium acts as inhibitor element in urolithiasis, its occurrence turns to be useful for the treatment and prevention of kidney stones [76].

Most of the calcium comes from Daily Dietary Intakes (DDI), especially from hard waters. Nevertheless, during the interview all the patients reported to drink mostly bottled water, except for patient KS022B (producer of uric acid stone), drinking only local tap water. It is worth to note that the fraction of calcium in the CaOx species is particularly higher than that expected for COD (ca. 24 wt.%) or COM (ca. 27 wt.%), and mainly follows the stoichiometric composition of anhydrous calcium oxalate (namely, ca. 31 wt.%). According to literature [20,55,83,87,88], whewellite is the most common and stable calcium oxalate that can be formed by partial dehydration of weddellite. This process could give rise to a perfect pseudomorphism [83], as observable for bipyramidal crystal inclusions in brushite aggregate KS006B. It is possible that oxalates in bladder stones can evolve to more stable (i.e., more anhydrous) phases, probably thanks to the dry conditions allowed by the internal and more compact parts of these aggregates, especially observed in the jackstone calculus KS012B.

Trace elements have been encountered in the CaP phases as a consequence of the isomorphic substitutions. Among them, metals such as sodium, iron, magnesium, zinc and potassium reach the highest values (**Fig. BOXPLOT**). The role of some of these metals in lithogenesis, for example zinc and iron, is still debated, whereas undesired trace elements such as copper, cadmium, lead, chromium, mercury and arsenic are generally attributable to environmental pollution or contaminated food. As a matter of fact, some of these elements (i.e., Hg, Cu and Cd) can cause important healthy problems, especially in kidney damage [30,86,89]. In the present study, Pb was detected in all the examined samples and its average elemental concentration (ca. 480 wt ppm) is consistent with that reported in the literature for Basilicata region (southern Italy) [30], as well as average concentrations of Cr found both in CaOx and uricite minerals. Another dangerous element, Hg, is often observed in association with selenium and displays significantly high concentrations

(on average ca. 800 wt ppm). Mercury is toxic also at low concentrations and can occur in environment and in food chain rarely as inorganic form (e.g., native Hg) or most commonly as organic form (mainly methylmercury or ethylmercury) [90]. The presence in the human body is also known to be ascribed to the dental amalgam restoration.

The role of selenium as inhibitor in urinary stones formation has been clearly highlighted in literature [7]. Selenium is considered an essential trace element for human body and its simultaneous occurrence with Hg seems to be mainly attributable to a methylmercury detoxification process, often leading to the formation of a rare HgSe compound known as tiemannite, recently found as small inclusion (< 10 μm) in a struvite bladder stone, surgically removed from a 4-years old Austrian patient [90]. We detected the tiemannite *via* EMPA, and considered the conditions of crystallization of this mineral as consistent with those required for struvite precipitation, namely low temperature (i.e., human body) and high pH values. In our investigation, Hg and Se were found in uric acid bladder stones (with stoichiometric ratio 1/1 with wt.% 70/30) that usually form in low pH urine, also compatible with the formation of tiemannite [90,91]. Therefore, we do not exclude that Hg and Se detected in the present study could be related to the occurrence of tiemannite tiny crystals.

The amount of Cu appears significantly lower than data from literature and is mainly observed in uric acid uroliths. Lastly, according to the literature [7], arsenic is often associated with antimony. The latter can accumulate in the human body displacing essential elements and acting as toxin [92].

From a clinical point of view, it is possible to consider the main causes that could lead to the formation of the examined bladder stones (Table Y). Except for the sample with brushite (KS006B) which suggests an idiopathic nature [11], for all the others it can be assumed that the cause is a condition of urine stasis due to potential obstructions of the urinary tract, favoring the considerable accumulation and consequent growth of these aggregates. Moreover, epistemological questionnaires report that patients daily consume alcohol, protein-rich (e.g., meats, eggs, cheeses) and oxalates-rich (e.g., coffee, cocoa, dried fruit) foods, all likely concurring to generate supersaturated urine which

may lead to the precipitation of uric acids and calcium oxalates, especially if associated to particularly low pH values.

Table Y. Synoptic table reporting classification of bladder stones examined in the present study and main clinical assumption.

n	ID_sample	Type*	Dominant phases	Minor Phases	Undesired elements	**Clinical assumption** [6,11]
1	KS006B	IVd	Brushite	CaOx, CaP	Hg, Pb, Sb, Cd, Cr	Idiopathic, potential exposure to pollution
2	KS011B	IIIa	Uric acid	CaOx	Hg, As, Pb, Sb, Cd, Cu	Eating and metabolic disorders, stasis, hyperuricosuria, hypercalciluria, potential exposure to pollution
3	KS012B	I/II	CaOx	CaP	Pb, Cd, Sb, Cu, Cr,	Hyperoxaluria, hypercalciluria, stasis, potential exposure to pollution
4	KS020B	IIIb	Uric acid	-	Hg, Pb, As, Se, Cd, Cu, Cr	Stasis, hyperuricosuria, potential exposure to pollution
5	KS022B	IIIa/IIIb	Uric acid	CaOx	Hg, Pb, Se, Cd, Cr	Stasis, low urine pH, hyperuricosuria, hypercalciluria, potential exposure to pollution
6	KS023B	IIIa	Uric acid	CaOx, CaP	Hg, Pb, As, Se, Cd, Cu, Cr	Stasis, hyperuricosuria, hypercalciluria, potential exposure to pollution

**, according to Daudon et al., 2016*

5. Conclusions

This multidisciplinary study has led to the characterization and classification of human bladder stones (including a jackstone calculus) of patients residing in the Campania region. As similar studies were not so far reported in the open literature, this contribution sheds new light on the potential clinical assumptions and some implications in the geohealth sphere, linked to the presence of some specific undesired elements. A brand-new finding worth to be underlined is that the distribution of the investigated chemical elements was regulated by each single mineralogical species that contributes to the urinary stones formation. This leads us to believe that an evaluation of the type and content of major and trace elements cannot be only achieved by means of wet chemical analysis (i.e., bulk chemical analysis). Actually, these techniques (e.g., Atomic Absorption Spectroscopy, AAS; Inductively Coupled Plasma, ICP) require a total destruction of the sample by digestion and provide chemical data representative of the entire stone sample. By contrast, the use of microscopic techniques coupled with microanalysis, such as those used for this study (i.e., EMPA/WDS) or others (e.g., LA-ICP-MS) [93], allows to investigate the sample, without destroying it, in a short time and with an acceptable limits of detection. The added value to our scientific and analytical approach is that we can discriminate the mineralogical species where these

elements tend to concentrate, for example by isomorphic substitution. **Table EMPA** shows the concentrations of the investigated elements (Na, K, Mg, Ca, Sr, Cr, Mn, Fe, Ni, Cu, Zn, Cd, Hg, Al, Sb, Pb, As, Se, P) in each mineralogical species of each sample. Excluding the most abundant elements (mainly Ca and P), all the others occur in the range of about one percent in weight. There is, therefore, a dualism in the partitioning of the elements in the mineralogical species belonging to the investigated urinary stones. The clearest interpretation is to consider calcium and phosphorus as the elements generating inorganic bladder stones, coming from the DDI and influencing the distribution of all the others trace elements. The concentrations of trace elements as a function of DDI have been addressed in several papers [20 and references therein]. Some are related to studies carried out on sedentary populations (e.g., Iran, Jordan) [19,29], which therefore return a fairly realistic representation of the contamination induced by the ingestion of food mostly consisting of ingredients (water, milk and dairy, vegetables, meat, etc.) from the areas where they live. In contrast, a very different situation occurs in Western populations, like the one resident in the Campania region, where the foods are not all indigenous, and, thus, infinite variables do not allow to univocally associate anomalous concentrations of trace elements to the territory in which the patient lives. In this study, the clinical interviews clearly indicate that the majority of patients drink bottled water and wine, the origin of which are unknown, and probably ascribable to areas far from their residence. At present, it is therefore not possible to make robust correlations between the geological environment hosting the patient and the presence of undesired elements. It is necessary to promote further studies that take into consideration a wider set of urinary stones (bladder, kidney stones) in order to increase the number of cases necessary to provide a statistically robust research. Above all, the combined use of wet chemical analysis (AAS, ICP) and EMPA/WDS must be envisaged for the purposes of dosing the trace elements and to satisfy two requests: how much is there and where the element is going to be concentrated.

Finally, the involvement of further expertise such as physiologists and nephrologists will be able to dispel the uncertainty regarding the possibility of understanding the mechanisms of

biominerogenesis and the way and timing of accumulation of undesired elements (i.e. Hg, As, Pb, Cd) during the nucleation and growth of this impacting biominerals.

Acknowledgements

ELETTRA Sincrotrone Trieste is thanked for the allocation of the beam-time, and Paolo Lotti for the assistance during the XRD data collection. Andrea Risplendente is thanked for the assistance during the EMPA/WDS analysis.

Antonia Cinelli

Valentina Materazzo

Altro…

References

[1] M.E. Moran, Urolithiasis: A Comprehensive History, 1st ed., Springer, 2014.

[2] E. V. Wilson, M.J. Bushiri, V.K. Vaidyan, Characterization and FTIR spectral studies of human urinary stones from Southern India, Spectrochim. Acta - Part A Mol. Biomol. Spectrosc. 77 (2010) 442–445. doi:10.1016/j.saa.2010.06.014.

[3] G. Schubert, Stone analysis, Urol. Res. 34 (2006) 146–150. doi:10.1007/s00240-005-0028-y.

[4] V. Kumar, G. Farell, S. Yu, S. Harrington, L. Fitzpatrick, E. Rzewuska, V.M. Miller, J.C. Lieske, Cell biology of pathologic renal calcification: contribution of crystal transcytosis, cell-mediated calcification, and nanoparticles, J. Investig. Med. 54 (2006) 412–424.

[5] A. Basiri, M. Taheri, F. Taheri, What is the state of the stone analysis techniques in urolithiasis?, Urol. J. 9 (2012) 445–454. doi:10.22037/uj.v9i2.1469.

[6] J. Cloutier, L. Villa, O. Traxer, M. Daudon, Kidney stone analysis: "Give me your stone, I will tell you who you are!," World J. Urol. 33 (2015) 157–169. doi:10.1007/s00345-014-1444-9.

[7] V.K. Singh, P.K. Rai, Kidney stone analysis techniques and the role of major and trace elements on their pathogenesis: a review, Biophys. Rev. 6 (2014) 291–310. doi:10.1007/s12551-014-0144-4.

[8] P. Chatterjee, A. Chakraborty, A.K. Mukherjee, Phase composition and morphological characterization of human kidney stones using IR spectroscopy, scanning electron microscopy and X-ray Rietveld analysis, Spectrochim. Acta - Part A Mol. Biomol. Spectrosc. 200 (2018) 33–42. doi:10.1016/j.saa.2018.04.005.

[9] L.W. Klee, C.G. Brito, J.E. Lingeman, The clinical implications of brushite calculi, J. Urol. 145 (1991) 715–718. doi:10.1016/S0022-5347(17)38432-X.

[10] A. Primiano, S. Persichilli, G. Gambaro, P.M. anue. Ferraro, A. D'Addessi, A. Cocci, A. Schiattarella, C. Zuppi, J. Gervasoni, FT-IR analysis of urinary stones: a helpful tool for clinician comparison with the chemical spot test, Dis. Markers. (2014) 5.

doi:10.1155/2014/176165.

[11] M. Daudon, A. Dessombz, V. Frochot, E. Letavernier, J.P. Haymann, P. Jungers, D. Bazin, Comprehensive morpho-constitutional analysis of urinary stones improves etiological diagnosis and therapeutic strategy of nephrolithiasis, Comptes Rendus Chim. 19 (2016) 1470–1491. doi:10.1016/j.crci.2016.05.008.

[12] E.L. Prien, C. Frondel, Studies in urolithiasis; the composition of urinary calculi., J. Urol. 57 (1947) 949–991. doi:10.1016/s0022-5347(17)69732-5.

[13] M.S. Ansari, N.P. Gupta, Impact of socioeconomic status in etiology and management of urinary stone disease, Urol. Int. 70 (2003) 255–61. doi:10.1159/000070130.

[14] M.L. Giannossi, G. Mongelli, F. Tateo, V. Summa, Mineralogical and morphological investigation of kidney stones of a Mediterranean region (Basilicata, Italy), J. Xray. Sci. Technol. 20 (2012) 175–186.

[15] B. Keshavarzi, N.Y. Ashayeri, F. Moore, D. Irani, S. Asadi, A. Zarasvandi, M. Salari, Mineralogical composition of urinary stones and their frequency in patients: Relationship to gender and age, Minerals. 6 (2016) 131. doi:10.3390/min6040131.

[16] A.H. Afaj, M.A. Sultan, Mineralogical composition of the urinary stones from different provinces in Iraq, ScientificWorldJournal. 5 (2005) 24–38. doi:10.1100/tsw.2005.2.

[17] G.C. Curhan, W.C. Willett, E.B. Rimm, F.E. Speizer, M.J. Stampfer, Body size and risk of kidney stones., J. Am. Soc. Nephrol. 9 (1998) 1645–1652.

[18] B. Hornberger, M.R. Bollner, Kidney stones, Physician Assist. Clin. 3 (2018) 37–54.

[19] I.A. Abboud, Mineralogy and chemistry of urinary stones: Patients from North Jordan, Environ. Geochem. Health. 30 (2008) 445–463. doi:10.1007/s10653-007-9128-7.

[20] M.L. Giannossi, Studio di biominerali patologici presenti nel corpo umano: caratteri composizionali ed influenza ambientale nel caso studio della Basilicata, Consiglio Regionale della Basilicata, 2013.

[21] D.R. Basavaraj, C.S. Biyani, A.J. Browning, J.J. Cartledge, The Role of Urinary Kidney

Stone Inhibitors and Promoters in the Pathogenesis of Calcium Containing Renal Stones{A figure is presented}, EAU-EBU Updat. Ser. 5 (2007) 126–136. doi:10.1016/j.eeus.2007.03.002.

[22] M. Sivaguru, J.J. Saw, J.C. Williams, J.C. Lieske, A.E. Krambeck, M.F. Romero, N. Chia, A.L. Schwaderer, R.E. Alcalde, W.J. Bruce, D.E. Wildman, G.A. Fried, C.J. Werth, R.J. Reeder, P.M. Yau, R.A. Sanford, B.W. Fouke, Geobiology reveals how human kidney stones dissolve in vivo, Sci. Rep. 8 (2018) 13731. doi:10.1038/s41598-018-31890-9.

[23] M.L. Giannossi, V. Summa, A Review of Pathological Biomineral Analysis Techniques and Classification Schemes, in: A. Cumhur (Ed.), An Introd. to Study Mineral., 2012: pp. 123–146. doi:10.5772/34861.

[24] A.I. Ancharov, S.S. Potapov, T.N. Moiseenko, I. V Feofilov, A.I. Nizovskii, Model experiment of in vivo synchrotron X-ray diffraction of human kidney stones, Nucl. Instruments Methods Phys. Res. Sect. A Accel. Spectrometers, Detect. Assoc. Equip. 575 (2007) 221–224.

[25] X. Li, R. Zhao, B. Liu, Y. Yu, Gemstone spectral imaging dual-energy computed tomography: a novel technique to determine urinary stone composition, Urology. 81 (2013) 727–730.

[26] F.A. Shiekh, M. Khullar, S.K. Singh, Lithogenesis: induction of renal calcifications by nanobacteria, Urol. Res. 34 (2006) 53–57.

[27] A.K. Mukherjee, Human kidney stone analysis using X-ray powder diffraction, J. Indian Inst. Sci. 94 (2014) 35–44.

[28] C.G.R. Nair, K.N. Ninan, Thermal decomposition studies: Part X. Thermal decomposition kinetics of calcium oxalate monohydrate—correlations with heating rate and samples mass, Thermochim. Acta. 23 (1978) 161–169.

[29] B. Keshavarzi, N. Yavarashayeri, D. Irani, F. Moore, A. Zarasvandi, M. Salari, Trace elements in urinary stones: a preliminary investigation in Fars province, Iran, Environ.

Geochem. Health. 37 (2015) 377–389. doi:10.1007/s10653-014-9654-z.

[30] M.L. Giannossi, V. Summa, G. Mongelli, Trace element investigations in urinary stones: A preliminary pilot case in Basilicata (Southern Italy), J. Trace Elem. Med. Biol. 27 (2013) 91–97. doi:10.1016/j.jtemb.2012.09.004.

[31] S. Öhman, L. Larsson, H.-G. Tiselius, Clinical significance of phosphate in calcium oxalate renal stones, Ann. Clin. Biochem. 29 (1992) 59–63.

[32] J. Kuta, J. Machát, D. Benová, R. Červenka, J. Zeman, P. Martinec, Association of minor and trace elements with mineralogical constituents of urinary stones: A hard nut to crack in existing studies of urolithiasis, Environ. Geochem. Health. 35 (2013) 511–522.

[33] C. Türk, J.F. Donaldson, A. Neisius, A. Petrik, A. Skolarikos, K. Thomas, EAU Guideline: Bladder Stones, 2019. https://uroweb.org/guideline/bladder-stones/.

[34] S. Perlmutter, C.T. Hsu, P.A. Villa, D.S. Katz, Sonography of a human jackstone calculus, J. Ultrasound Med. 21 (2002) 1047–1051. doi:10.7863/jum.2002.21.9.1047.

[35] K.J. Singh, A. Tiwari, A. Goyal, Jackstone: A rare entity of vesical calculus, Indian J. Urol. (2011). doi:10.4103/0970-1591.91449.

[36] A.P. Sweeney, R.B. Dyer, The “jackstone” appearance, Abdom. Imaging. 40 (2015) 2906–2907. doi:10.1007/s00261-015-0440-x.

[37] B. B, F. F, F. FC, F. U, Jackstone Calculus: A Rare Subtype of Urinary Stone with a Sea-Urchin Appearance, Int. J. Nephrol. Kidney Fail. 4 (2019) 1–2. doi:10.16966/2380-5498.166.

[38] P. Lotti, S. Milani, M. Merlini, B. Joseph, F. Alabarse, A. Lausi, Single-crystal diffraction at the high-pressure Indo-Italian beamline Xpress at Elettra, Trieste https://orcid.org/0000-0003-2272-8281 Lotti Paolo, J. Synchrotron Radiat. 27 (2020) 222–229. doi:10.1107/S1600577519015170.

[39] A.P. Hammersley, FIT2D: A multi-purpose data reduction, analysis and visualization program, J. Appl. Crystallogr. 49 (2016) 646–652. doi:10.1107/S1600576716000455.

[40] N. Abrol, N.S. Kekre, Revisiting Randall’s plaque, African J. Urol. 20 (2014) 174–179.

doi:10.1016/j.afju.2014.06.001.

[41] E. Letavernier, D. Bazin, M. Daudon, Randall's plaque and kidney stones: Recent advances and future challenges, Comptes Rendus Chim. 19 (2016) 1456–1460. doi:10.1016/j.crci.2014.12.005.

[42] N. Çiftçioğlu, K. Vejdani, O. Lee, G. Mathew, K.M. Aho, E.O. Kajander, D.S. McKay, J.A. Jones, M.L. Stoller, Association between Randall's plaque and calcifying nanoparticles, Int. J. Nanomedicine. 3 (2008) 105.

[43] mindat.org, (n.d.). https://www.mindat.org/min-4276.html.

[44] mindat.org, (n.d.). https://www.mindat.org/min-793.html.

[45] H. Ringertz, Optical and crystallographic data of uric acid and its dihydrate, Acta Crystallogr. 19 (1965) 286. doi:10.1107/s0365110x65003298.

[46] S. Gràcia-Garcia, F. Millán-Rodríguez, F. Rousaud-Barón, R. Montañés-Bermúdez, O. Angerri-Feu, F. Sánchez-Martín, H. Villavicencio-Mavrich, A. Oliver-Samper, Why and how we must analyze urinary calculi, Actas Urológicas Españolas. 35 (2011) 354–362. doi:10.1016/j.acuroe.2011.01.005.

[47] L. Muschietti, V. Orto, G. Garrido, Infrared Spectroscopic Analysis of Urinary Calculi: A Retrospective Study in Argentinean Patients, Asian J. Med. Heal. 1 (2016) 1–9. doi:10.9734/ajmah/2016/29354.

[48] E. Schnitzler, M. Kobelnik, G.F.C. Sotelo, G. Bannach, M. Ionashiro, Thermoanalytical study of purine derivatives compounds, Eclet. Quim. 29 (2004) 71–78. doi:10.1590/S0100-46702004000100009.

[49] K. Sekkoum, A. Cheriti, S. Taleb, N. Belboukhari, FTIR spectroscopic study of human urinary stones from El Bayadh district (Algeria), Arab. J. Chem. 9 (2016) 330–334. doi:10.1016/j.arabjc.2011.10.010.

[50] R. Selvaraju, A. Raja, G. Thiruppathi, FT-IR spectroscopic, thermal analysis of human urinary stones and their characterization, Spectrochim. Acta - Part A Mol. Biomol. Spectrosc.

137 (2015) 1397–1402. doi:10.1016/j.saa.2014.09.046.

[51] A. Aslin Shamema, K. Thanigai Arul, R. Senthil Kumar, S.N. Kalkura, Physicochemical analysis of urinary stones from Dharmapuri district, Spectrochim. Acta - Part A Mol. Biomol. Spectrosc. 134 (2015) 442–448. doi:10.1016/j.saa.2014.05.088.

[52] S. Mandel, A.C. Tas, Brushite (CaHPO4·2H2O) to octacalcium phosphate (Ca8(HPO4)2(PO4)4·5H2O) transformation in DMEM solutions at 36.5 °C, Mater. Sci. Eng. C. 30 (2010) 245–254. doi:10.1016/j.msec.2009.10.009.

[53] V.B. Suryawanshi, R.T. Chaudhari, Growth and Characterization of Agar Gel Grown Brushite Crystals, Indian J. Mater. Sci. (2014) 6. doi:10.1155/2014/189839.

[54] A. Hirsch, I. Azuri, L. Addadi, S. Weiner, K. Yang, S. Curtarolo, L. Kronik, Infrared absorption spectrum of brushite from first principles, Chem. Mater. 26 (2014) 2934–2942. doi:10.1021/cm500650t.

[55] C. Conti, L. Brambilla, C. Colombo, D. Dellasega, G.D. Gatta, M. Realini, G. Zerbi, Stability and transformation mechanism of weddellite nanocrystals studied by X-ray diffraction and infrared spectroscopy, Phys. Chem. Chem. Phys. 12 (2010) 14560–14566. doi:10.1039/c0cp00624f.

[56] G. Kanchana, P. Sundaramoorthi, G.P. Jeyanthi, Bio-Chemical Analysis and FTIR-Spectral Studies of Artificially Removed Renal Stone Mineral Constituents, J. Miner. Mater. Charact. Eng. 8 (2009) 161–170. doi:10.4236/jmmce.2009.82014.

[57] A. Le Bail, H. Duroy, J.L. Fourquet, Ab-initio structure determination of LiSbWO6 by X-ray powder diffraction, Mater. Res. Bull. 23 (1988) 447–452. doi:10.1016/0025-5408(88)90019-0.

[58] M. Afzal, M. Iqbal, H. Ahmad, Thermal analysis of renal stones, J. Therm. Anal. 38 (1992) 1671–1682. doi:10.1007/BF01979363.

[59] M. Berényi, G. Liptay, The use of thermal analysis in medical science with special reference to nephroliths, J. Therm. Anal. 3 (1971) 437–443. doi:10.1007/BF02188652.

[60] R.L. Frost, M.L. Weier, K.L. Erickson, Thermal decomposition of struvite: Implications for the decomposition of kidney stones, J. Therm. Anal. Calorim. 76 (2004) 1025–1033. doi:10.1023/B:JTAN.0000032287.08535.b3.

[61] A. Kohutova, P. Honcova, V. Podzemna, P. Bezdicka, E. Vecernikova, M. Louda, J. Seidel, Thermal analysis of kidney stones and their characterization, J. Therm. Anal. Calorim. 101 (2010) 695–699. doi:10.1007/s10973-010-0914-6.

[62] H.P. Lee, D. Leong, C.T. Heng, Characterization of kidney stones using thermogravimetric analysis with electron dispersive spectroscopy, Urol. Res. 40 (2012) 197–204. doi:10.1007/s00240-011-0428-0.

[63] A.R. Izatulina, V. V. Gurzhiy, M.G. Krzhizhanovskaya, N. V. Chukanov, T.L. Panikorovskii, Thermal behavior and phase transition of uric acid and its dihydrate form, the common biominerals uricite and tinnunculite, Minerals. 9 (2019) 373. doi:10.3390/min9060373.

[64] S. Popescu, M. Stefanescu, E. Popovici, I. Perhaita, Evaluation of the renal calculi compositions: Thermal and FT-IR analysis, J. Therm. Anal. Calorim. 114 (2013) 765–775. doi:10.1007/s10973-013-3033-3.

[65] M. Galván-Ruiz, J. Hernández, L. Baños, J. Noriega-Montes, M.E. Rodríguez-García, Characterization of Calcium carbonate, calcium oxide, and calcium hydroxide as starting point to the improvement of lime for their use in construction, J. Mater. Civ. Eng. 21 (2009). doi:10.1061/(ASCE)0899-1561(2009)21:11(694).

[66] L. Berzina-Cimdina, N. Borodajenko, Research of Calcium Phosphates Using Fourier Transform Infrared Spectroscopy, in: Infrared Spectrosc. - Mater. Sci. Eng. Technol., 2012: pp. 123–148. doi:10.5772/36942.

[67] F. Izzo, C. Germinario, C. Grifa, A. Langella, M. Mercurio, External reflectance FTIR dataset (4000–400 cm−1) for the identification of relevant mineralogical phases forming Cultural Heritage materials, Infrared Phys. Technol. 106 (2020) 103266.

doi:10.1016/j.infrared.2020.103266.

[68] K. Lawson-Wood, I. Robertson, Study of the Decomposition of Calcium Oxalate Monohydrate using a Hyphenated Thermogravimetric Analyser - FT-IR System (TG-IR), (2016) 3. https://www.perkinelmer.com/lab-solutions/resources/docs/APP_Decomposition_Calcium Oxalate_Monohydrate(013078_01).pdf.

[69] A. Dosen, R.F. Giese, Thermal decomposition of brushite, CaHPO4·2H2O to monetite CaHPO4 and the formation of an amorphous phase, Am. Mineral. 96 (2011) 368–373,. doi:10.2138/am.2011.3544.

[70] S. Fiore, R. Laviano, Brushite, hydroxylapatite, and taranakite from Apulian caves (southern Italy): New mineralogical data, Am. Mineral. 76 (1991) 1722–1727.

[71] S. Jmai, M. Bagane, M. Queneudec-T'kint, Physico-chemical, thermal, thermodynamic and kinetic characterization of a porous material (Di-calcium phosphate), Heat Mass Transf. Und Stoffuebertragung. 55 (2019) 3589–3602. doi:10.1007/s00231-019-02625-x.

[72] R. Mulongo-Masamba, T. El Kassri, M. Khachani, S. Arsalane, M. Halim, A. El Hamidi, Synthesis and thermal dehydroxylation kinetic of anhydrous calcium phosphate monetite CaHPO4, J. Therm. Anal. Calorim. 124 (2016) 171–180. doi:10.1007/s10973-015-5130-y.

[73] F. Grases, A. Costa-Bauzá, L. García-Ferragut, Biopathological crystallization: a general view about the mechanisms of renal stone formation, Adv. Colloid Interface Sci. 74 (1998) 169–194. doi:https://doi.org/10.1016/S0001-8686(97)00041-9.

[74] C. Türk, A. Petřík, K. Sarica, C. Seitz, A. Skolarikos, M. Straub, T. Knoll, EAU Guidelines on Interventional Treatment for Urolithiasis, 2016. doi:10.1016/j.eururo.2015.07.041.

[75] C.J. Wang, C.S. Hsu, H.W. Chen, P.C. Tsai, C.H. Chang, Long-Term Effects of Lemonade Therapy on Hypocitraturic Nephrolithiasis and Stone Recurrence: A Mini Review, Int J Nephrol Kidney Fail. 2 (2016) 1–4.

[76] L. Frassetto, I. Kohlstadt, Treatment and prevention of kidney stones: An Update, Am. Fam.

Physician. 84 (2011) 1234–1242.

[77] A.P. Evan, J.E. Lingeman, F.L. Coe, Y. Shao, J.H. Parks, S.B. Bledsoe, C.L. Phillips, S. Bonsib, E.M. Worcester, A.J. Sommer, S.C. Kim, W.W. Tinmouth, M. Grynpas, Crystal-associated nephropathy in patients with brushite nephrolithiasis, Kidney Int. 67 (2005) 576–591. doi:10.1111/j.1523-1755.2005.67114.x.

[78] C. Hill, P. Forti, Cave minerals of the world, 2nd ed., National Speleological Society, 1997.

[79] C.G. Rivell, J.S. Coren, Onesies, Twosies, not a game of Jackstones, Osteopath. Fam. Physician. 4 (2012) 88–90. doi:10.1016/j.osfp.2011.10.002.

[80] S. Goonewardena, U. Jayarajah, S.N. Kuruppu, M.H. Fernando, Jackstone in the Kidney: An Unusual Calculus, Case Rep. Urol. (2021) 3. doi:10.1155/2021/8816547.

[81] D. Subasinghe, S. Goonewardena, V. Kathiragamathamby, Jack stone in the bladder: case report of a rare entity, BMC Urol. 17 (2017) 40. doi:10.1186/s12894-017-0230-6.

[82] B. Brogna, F. Flammia, F.C. Flammia, U. Flammia, A Large Jackstone Calculus Incidentally Detected on CT Examination: A Case Report With Literature Review, World J. Nephrol. Urol. 7 (2018) 85–87. doi:10.14740/wjnu372.

[83] R.I. Gibson, Descriptive human pathological mineralogy, Am. Mineral. J. Earth Planet. Mater. 59 (1974) 1177–1182.

[84] M.L. Giannossi, La geologia in difesa della salute: nuovi sbocchi professionali, Geol. Territ. Ambient. 7 (2010) 3–9.

[85] L. Wang, M. Chen, P. He, H. Yu, K.A. Block, Z. Xie, Composition and spatial distribution of elements and isotopes of a giant human bladder stone and environmental implications, Sci. Total Environ. 650 (2019) 835–846.

[86] J. Kuta, J. Machát, D. Benová, R. Červenka, T. Kořistková, Urinary calculi - Atypical source of information on mercury in human biomonitoring, Cent. Eur. J. Chem. 10 (2012) 1475–1483. doi:10.2478/s11532-012-0063-9.

[87] D. Bazin, C. Leroy, F. Tielens, C. Bonhomme, L. Bonhomme-Coury, F. Damay, D. Le

Denmat, J. Sadoine, J. Rode, V. Frochot, Hyperoxaluria is related to whewellite and hypercalciuria to weddellite: What happens when crystalline conversion occurs?, Comptes Rendus Chim. 19 (2016) 1492–1503.

[88] W. Zhao, N. Sharma, F. Jones, P. Raiteri, J.D. Gale, R. Demichelis, Anhydrous calcium oxalate polymorphism: A combined computational and synchrotron X-ray diffraction study, Cryst. Growth Des. 16 (2016) 5954–5965.

[89] N.A. Pal'chik, T.N. Moroz, N. V. Maksimova, A. V. Dar'in, Mineral and microelement compositions of urinary stones, Russ. J. Inorg. Chem. 51 (2006) 1098–1105. doi:10.1134/S0036023606070138.

[90] R. Moser, F. Zaccarini, T. Alber, R. Kerbl, First finding of tiemannite, HgSe, in human bladder stones: An electron microprobe study, Micron. 138 (2020) 102928.

[91] R.M. Hazen, J. Golden, R.T. Downs, G. Hystad, E.S. Grew, D. Azzolini, D.A. Sverjensky, Mercury (Hg) mineral evolution: A mineralogical record of supercontinent assembly, changing ocean geochemistry, and the emerging terrestrial biosphere, Am. Mineral. 97 (2012) 1013–1042.

[92] M. Słojewski, Major and trace elements in lithogenesis, Cent. Eur. J. Urol. 64 (2011) 58.

[93] M.A. Chaudhri, J. Watling, F.A. Khan, Spatial distribution of major and trace elements in bladder and kidney stones, J. Radioanal. Nucl. Chem. 271 (2007) 713–720.

Figure captions

Fig. SM – Micrographs of bladder stones captured in stereomicroscopy: a) and b) KS006B; c) KS011B; d) and e) KS012B; f), g) and h) KS020; i) and j) KS022B; k) and l) KS023B.

Fig. SM – Micrographs of bladder stones captured in polarized light microscopy: a) internal structure and b) detail of calcium oxalate crystals for sample KS012B; c)

Fig. FTIR – FTIR spectra of analyzed bladders: KS006B (brushite), KS011B (uric acid), KS012B (calcium oxalate) KS020 (uric acid), KS022B (uric acid) and KS023B (uric acid).

Fig. STA – Thermal analyses and EGA-FTIR of UA (KS011B), COM (KS012B) and brushite + COM (KS006B).